Journal of The Electrochemical Society, **152** (4) A716-A720 (2005)
0013-4651/2005/152(4)/A716/5/$7.00 © The Electrochemical Society, Inc.

Characteristics and Electrochemical Performance of Supercapacitors with Manganese Oxide-Carbon Nanotube Nanocomposite Electrodes

Chia Ying Lee,[a] Huei Mei Tsai,[b] Huey Jan Chuang,[b] Seu Yi Li,[c] Pang Lin,[c] and Tseung Yuen Tseng[a,z]

[a]*Department of Electronics Engineering and Institute of Electronics, National Chiao Tung University, Hsinchu 300, Taiwan*
[b]*Materials and Electro-optics Research Division, Chung Shan Insititute of Science and Technology, Taoyuan 325, Taiwan*
[c]*Institute of Materials Science and Engineering, National Chiao Tung University, Hsinchu 300, Taiwan*

Supercapacitor characteristics of manganese oxide/nickel (MnO_x/Ni) and manganese oxide/carbon nanotubes/nickel (MnO_x/CNTs/Ni) nanocomposite electrodes were investigated in this study. The CNTs were deposited on the Ni substrate by electrophoresis in a 0.5 mg CNT/1 mL dimethylformamide solution, whereas the MnO_x were synthesized by anodic deposition in a 0.16 M manganese sulfate pentahydrate aqueous solution on substrates. The crystallinity and surface morphology of these electrodes were determined by X-ray diffraction, scanning electron microscopy, and transmission electron microscopy. The capacitive properties of these electrodes were demonstrated by cyclic voltammetry with scan rates ranging from 5 to 100 mV/s. The specific capacitances of the MnO_x/CNT/Ni nanocomposite electrode were 415 and 388 F/g with scan rates of 5 and 100 mV/s, respectively. After 1000 cycles of operation, this electrode can maintain 79% of its original capacitance. These MnO_x/CNT/Ni nanocomposite electrodes possessing good electrochemical reversibility and high capacitance may be appropriate for supercapacitor application in the future.
 [DOI: 10.1149/1.1870793]

Manuscript submitted September 8, 2004; revised manuscript received October 26, 2004.
Available electronically March 1, 2005.

With the development of technology, energy storage devices, including batteries[1] and supercapacitors,[2-7] have drawn much .attention for their potential applications in the power sources of various electronic products. The battery is a device that stores electrical energy by an electrochemical reaction, whereas the supercapacitor stores electrical energy by the physical adsorption and the reversible faradaic redox reaction taking place on the surface of a substrate material. Although the battery exhibits high energy density, electrochemical stability, and power density, it still requires improvement in the reversibility of chemical reactions. Worldwide attention is focused on supercapacitors due to their safety, short charging time, electrochemical stability, high power density, and long cycle life. These supercapacitors can be classified according to the charge storage mechanisms: the electric double-layer capacitor (EDLC)[3,4] and the faradaic capacitor.[5-7] The EDLC consists of a high specific surface material because the energy storage mechanism is the electronic and ionic charges physically adsorbed on the interface of the double layer. However, the faradaic capacitor consists of several oxidation states of material as the mechanism involves not only physical adsorption of electrons and ions, but also the reversible redox reactions occurring on the electrode surface.

Carbon nanotubes (CNTs) are attractive materials applied in energy storage devices, such as secondary batteries,[8] fuel cells,[9] and pseudocapacitors,[10-12] because of their chemical stability, low mass density, activated high surface area, and high conductivity. The specific capacitances of CNT-based electrodes have been reported to be between 4 and 146.6 F/g in a solution of H_2SO_4, which is relatively lower than that of an activated carbon electrode with large area. To provide enhanced capacitance, composite electrodes, such as activated carbon-indium-tin oxide,[13] polyaniline-gold nanoclusters,[14] and RuO_x-VO_2[15] are currently being investigated for supercapacitor applications. Park *et al.* reported that the RuO_x modification of CNTs provides a composite electrode material that shows a specific capacitance based on the mass of RuO_x, and the value is 900 F/g.[16] Therefore, suitably modified transition-metal oxide CNTs would form potential composite materials for use in the supercapacitors.

In this study, a manganese oxide-CNT composite electrode was investigated. The $MnO_x{\cdot}nH_2O$/Ni and $MnO_x{\cdot}nH_2O$/CNTs/Ni electrodes were synthesized by anodic deposition. The crystal structures, surface morphologies, and microstructures of these composite electrodes were investigated. The capacitance and rechargeable properties were characterized by the cyclic voltammetric method and constant current discharge method. An equivalent circuit model was proposed and demonstrated by an impedance analyzer.

Experimental

Electrode synthesis.—The 10×10 mm^2 nickel substrates (Nilaco, Japan) were etched with 20% HNO_3 solution at room temperature for 10 min to increase the roughness of the surface, cleaned with deionized (DI) water in an ultrasonic bath, and dried in a vacuum oven at 90°C for 24 h. To obtain CNTs with acidic sites on the surface, the CNTs were put in a boiling 70% nitric acid solution for 1 h[17] and dried in an oven at 90°C for 24 h before electrophoretic deposition (EPD). The EPD technique was adopted to deposit the CNTs on the Ni substrate.[18] The CNTs were dispersed by ultrasonic agitation in a bath of dimethylformamide with a concentration of 0.5 mg/mL. The nickel and platinum sheets were put in this solution as the cathode and the anode electrode, respectively. The CNTs were electrophoretically deposited on the Ni substrate after a direct current (dc) voltage of 20 V was applied for 5 min. Then the $MnO_x{\cdot}nH_2O$ films were deposited on the Ni and CNTs/Ni substrates by an anodic deposition with a platinum sheet as the counter electrode and saturated calomel electrode (SCE) as the reference electrode in a 0.16 M $MnSO_4{\cdot}5H_2O$ solution pH 5.6. Such an amorphous-$MnO_x{\cdot}nH_2O$ film was deposited by the potentiostatic method at 0.4 V for 3 min. The deposition condition was controlled by an EG&G Princeton Applied Research model 263 potentiometer. After deposition, the electrode was cleaned with DI water and dried in a vacuum oven at room temperature for 24 h.

Structural analysis.—The weight of the amorphous $MnO_x{\cdot}nH_2O$ films was determined by a microbalance with an accuracy of 10 μg. The crystal structure of these samples was examined by X-ray diffraction (XRD, MAC Science, MXP18, Japan) employing a Cu target at an angle speed of 4° (2θ) min^{-1}. The surface morphology and microstructure of these electrodes were studied by field-emission-scanning electron microscopy (FE-SEM, Hitachi S-4700I instru-

[z] E-mail: tseng@cc.nctu.edu.tw

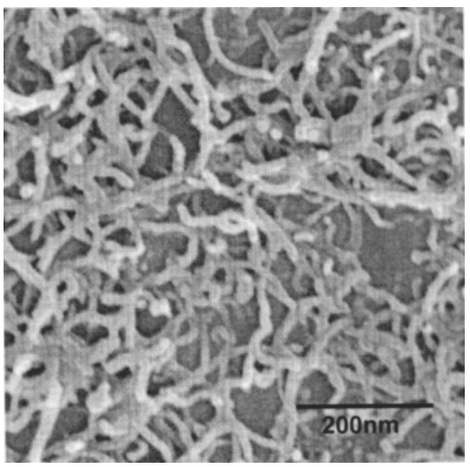

Figure 1. FE-SEM photograph of CNT/Ni surface.

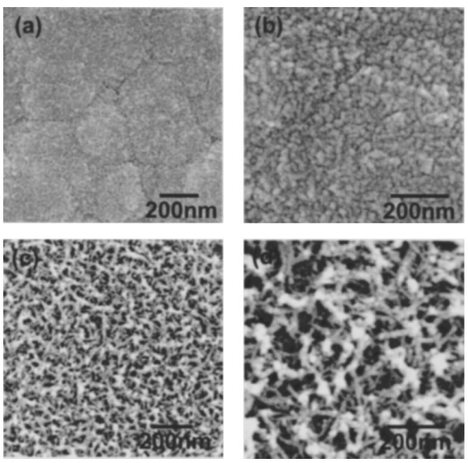

Figure 2. FE-SEM photographs of (a, b) MnO_x/Ni surface and (c,d) MnO_x/CNT/Ni surface.

ment, Japan) and high resolution transmission electron microscopy (HRTEM, Philips Tecnai 20 instrument) coupled with an energy dispersive X-ray analysis (EDX) spectrometer (Oxford, England). The measurement of surface area of the electrodes was carried out by the multipoint Brunauer, Emmett, and Teller method (BET, Quantachrome Instruments) using N_2 gas.

Electrochemical characterization of MnO_x/Ni and MnO_x/CNTs/Ni composite electrodes.—All the electrochemical testing was carried out in a three-compartment cell with a SCE reference electrode, a counter electrode of platinum sheet, and 0.1 M Na_2SO_4 as the electrolyte. Before electrochemical analysis, the cell was purged with argon atmosphere to remove the oxygen. Electrochemical characterizations of MnO_x/Ni and MnO_x/CNTs/Ni composite electrodes were demonstrated by a potenstiostat/galvanostat (EG&G Princeton Applied Research model 263) with the working voltage from 0 to 1 V at a scan rate varied from 5 to 100 mV/s. The constant current discharge (CCD) reaction was carried out chronopotentiometrically at a cathodic current of 0.1 mA after appling a positive potential bias of 1 V for 30 s. The capacitance can be calculated from the equation

$$c = \frac{i}{(dV/dt)} \qquad [1]$$

where c is the specific capacitance, i is the specific voltammetric charge within the working voltage, and V is the potential. The amplitude of the as- applied potential signal was 10 mV, and the frequency ranged from 10 mHz to 100 kHz.

Results and Discussion

Structural analysis of MnO_x/Ni and MnO_x/CNTs/Ni composite electrodes.—An FE-SEM image of the CNTs/Ni substrate is shown in Fig. 1, indicating that the CNTs electrophoretically deposited on the Ni substrate are of 20-30nm diam. These CNTs are randomly distributed, entangled, and cross-linked on the Ni substrate. The surface of the electrode becomes rough after CNT deposition. The evidence for this has been derived from the BET surface area measurements of the Ni and CNTs/Ni substrates, which are calculated as 0.7 and 14.9 m^2/g, respectively. The BET surface area increases with the deposition of the high-surface-area CNTs ($\sim$298.7 m^2/g based on the mass of CNTs only) on the Ni substrate.

Then the $MnO_x \cdot nH_2O$ films were anodic deposited on the Ni and CNTs/Ni substrates. The weights of these films measured by the microbalance were 20 and 18 μg, respectively. According to the XRD patterns (not shown here), the crystal structures of anodically deposited $MnO_x \cdot nH_2O$ films on the Ni and CNT/Ni substrates are amorphous. The FE-SEM images shown in Fig. 2 reveal the surface morphologies of the anodically deposited $MnO_x \cdot nH_2O$ films on the Ni and CNTs/Ni substrates. The surface morphologies of the $MnO_x \cdot nH_2O$ film grown on the Ni substrate (Fig. 2a and 2b) indicate a the relatively smooth surface of the film with an average particle size of 25 nm. However, the surface morphology of the MnO_x film on the CNTs/Ni substrate is different. As shown in Fig. 2c and 2d, it consists of 10-25 nm MnO_x primary and secondary (*i.e.*, agglomerates) nanoparticles on the substrate surface. The different MnO_x morphologies between the two substrates could be due to the different initial surface morphologies between Ni and CNTs/Ni substrates. The BET measured surface area of the MnO_x/Ni is 6.0 m^2/g, and the increasing surface area based on the mass of MnO_x only is 58.9 m^2/g. However, the BET measured surface area of the MnO_x/CNTs/Ni substrate is 20.2 m^2/g, and the increasing surface area based on the mass of MnO_x only is 82.0 m^2/g. The BET surface area of MnO_x/CNTs/Ni has been found to be larger than that of MnO_x/Ni due to the application of CNTs. Obviously, the MnO_x nanoparticles grown on the CNTs/Ni substrate have a larger surface area than that on the Ni substrate. Such a porous MnO_x film may provide a large redox reaction area to achieve fast charge/discharge rates.

To realize the influence of charge/discharge cycling on the morphologies of MnO_x on the substrate, the morphologies of the

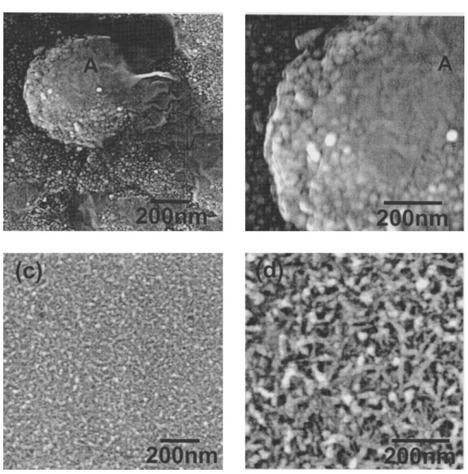

Figure 3. FE-SEM photographs of (a, b) MnO_x/Ni surface and (c,d) MnO_x/CNT/Ni surface after 100 cycles of CV testing.

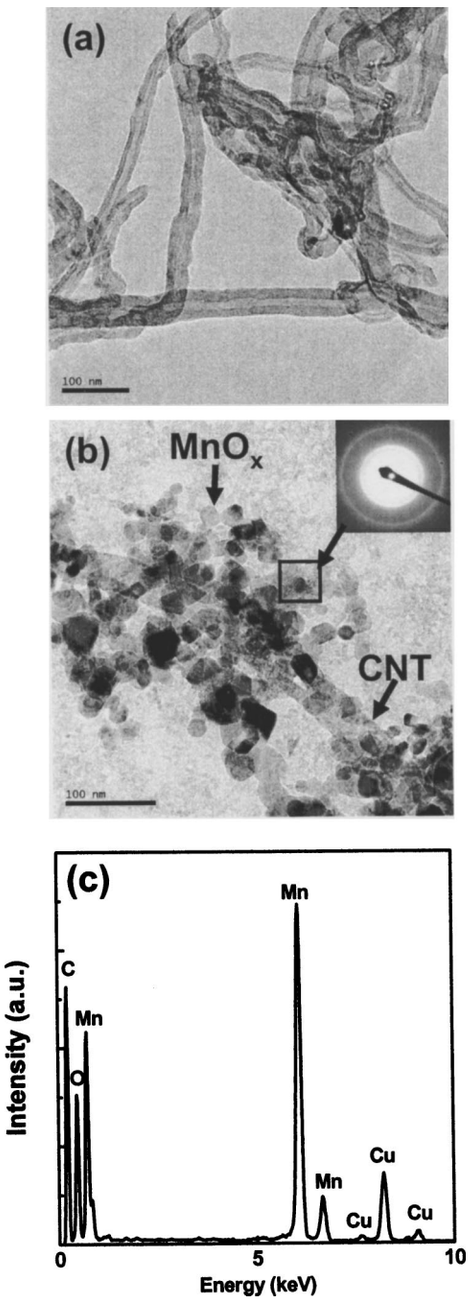

Figure 4. HRTEM images of (a) CNT and (b) MnO_x/CNT nanocomposite (inset is SAED of MnO_x nanoparticles). (c) EDX spectrum of MnO_x nanoparticles.

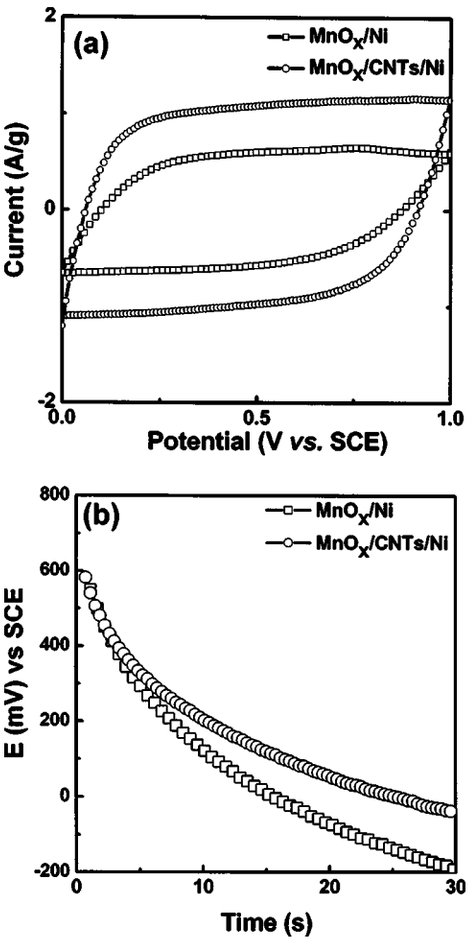

Figure 5. (a) CV curves for the a-MnO_x/Ni and a-MnO_x/CNTs/Ni electrodes in 0.1 M Na_2SO_4 solution at 25°C with a potential scan rate of 10 mV/s. (b) CCD curves for the a-MnO_x/Ni and a-MnO_x/CNTs/Ni electrodes.

MnO_x/Ni and MnO_x/CNTs/Ni films after 100 cycles of cyclic voltammetry (CV) measurements are observed and shown in Fig. 3. It is indicated in Fig. 3a and 3b that some of the amorphous MnO_x particles reveal a particle size of 45 nm on the Ni substrate, and others merge to larger secondary particles and a smoother surface (region A). The surface morphology of MnO_x/CNTs/Ni is shown in Figs. 3c and 3d after 100 cycles of CV measurement. Few MnO_x nanoparticles tend to detach from the surface, as the average diameter of MnO_x nanoparticles increases to 30 nm with an increase in the cycles of CV measurement, and no MnO_x particles merge into the larger ones like in region A. After such a CV cycling, the BET surface area of the MnO_x/Ni electrode changes to 3.36 m^2/g, and that of the MnO_x/CNTs/Ni electrode 19.83 m^2/g. Clearly, the reaction area of the MnO_x/Ni electrode has a larger reduction due to the change of surface morphologies. Therefore, the MnO_x/CNTs/Ni electrode would show the better reversibility because it has a-MnO_x nanoparticles grown on the CNTs/Ni substrate that could keep the smaller particles from merging into the larger ones after the CV cycles.

Figure 4 illustrates the HRTEM images of the CNT and anodically deposited MnO_x. It is indicated in Fig. 4a that the CNTs are all multiwall with an average diam of 20 nm. The MnO_x particles on the CNTs/Ni have diam ranging from 10 to 25 nm (Fig. 4b). The selected area electron diffraction (SAED) pattern (inset in Fig. 4b) of the MnO_x nanoparticle could not be indexed to any of the MnO_x lattice structures as these particles are all amorphous. The EDX spectrum, shown in Fig. 4c, of MnO_x nanoparticles determined by the EDX spectrometer attached to the transmission electron microscope, reveals that manganese (Mn) and oxygen (O) are the main constituents of the nanoparticles, while the Cu peak is generated by the Cu grid. It also shows that the chemical composition is nonstoichiometric manganese oxide, $MnO_{1.70}$, anodically deposited on the substrates.

Electrochemical characterizations of MnO_x/CNTs composite electrodes.—Figure 5a shows the CV curves of the MnO_x/Ni and MnO_x/CNTs/Ni composite electrodes in 0.1 M Na_2SO_4 solution at 25°C cycled under a potential in the range from 0 to 1.0 V

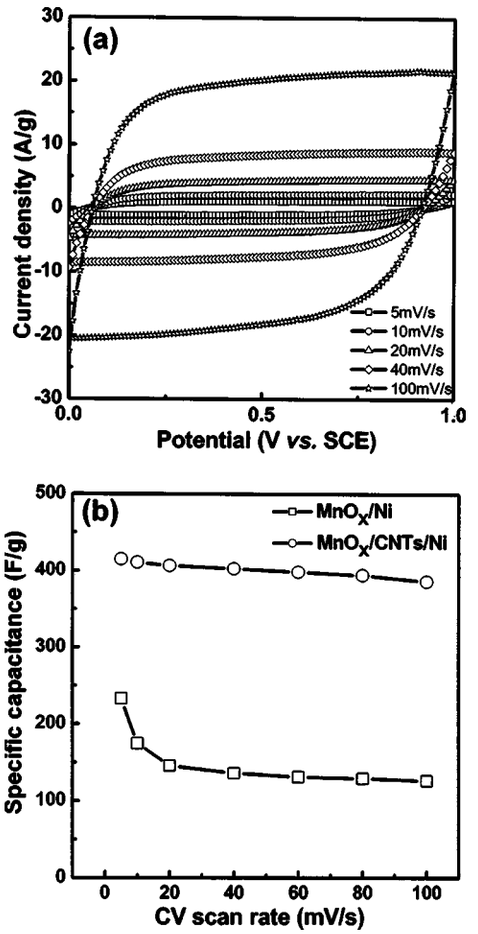

Figure 6. (a) Variation of CV curves of the a-MnO_x/CNTs/Ni electrode with potential scan rates as indicated. (b) Variation of specific capacitances of a-MnO_x/Ni and a-MnO_x/CNTs/Ni electrodes with CV scan rate.

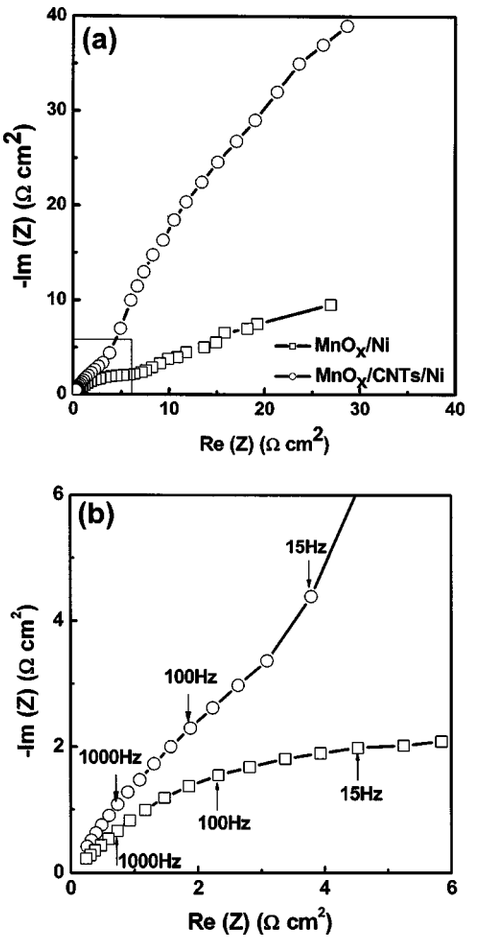

Figure 7. (a) Nyquist impedance spectra of a-MnO_x/Ni and a-MnO_x/CNTs/Ni electrodes measured at OCP (10 mV *vs.* SCE). (b) The impedance spectra in the high-frequency region.

with a scan rate of 5 mV/s. Both the CV curves are almost rectangular in shape, which implies that both of them exhibit capacitive behavior. The mean specific capacitances of the MnO_x/Ni and MnO_x/CNTs/Ni composite electrodes based on the mass of MnO_x (Fig. 5a) are 233 and 415 F/g, respectively. The CCD curves of the MnO_x/Ni and MnO_x/CNTs/Ni composite electrodes indicated in Fig. 5b depict that the slopes for both curves are not constant. The average specific capacitances of the MnO_x/Ni and MnO_x/CNTs/Ni electrodes calculated from the average slope based on Eq. 1 are 241 and 418 F/g, respectively. The larger specific capacitance existing in the MnO_x/CNTs/Ni electrode may be attributed to the porous surface of this electrode providing a larger surface area between the aqueous electrolyte and the MnO_x nanoparticles to facilitate redox reaction. This suggestion could be demonstrated by the CV measurements with various scan rates. The effect of scan rate on the CV curves of the MnO_x/CNTs/Ni electrode is shown in Fig. 6a. All the curves are almost rectangular and show a capacitive behavior. The mean specific capacitances of MnO_x/CNTs/Ni with scan rates of 10, 20, 40, and 100 mV/s are 410, 407, 403, and 386 F/g, respectively. These CV curves demonstrate that the anodically deposited MnO_x/CNTs/Ni composite electrode has excellent redox reversibility. Figure 6b shows the influence of potential scan rate on the capacitance recorded with scan rates from 5 to 100 mV/s for the MnO_x/Ni and MnO_x/CNTs/Ni composite electrodes. The specific capacitances at the scan rate of 5 mV/s calculated from the CV curves of these two electrodes are the highest, 233 (MnO_x/Ni) and 415 (MnO_x/CNTs/Ni) F/g. As shown in the figure, the specific capacitances of these electrodes decrease as the potential scan rate increases. As the potential scan rate is raised to 100 mV/s, the specific capacitance of the MnO_x/Ni electrode decreases to 126 F/g, which is 54% of that measured with a scan rate of 5 mV/s, whereas the specific capacitance of MnO_x/CNTs/Ni is 386 F/g, which is 93% of that measured with a scan rate of 5 mV/s. The MnO_x/CNTs/Ni electrode exhibits good reaction reversibility and less capacitance decay for faster potential scan rates, probably due to the high conductivity of CNTs, which act as a good current collector with a low contact resistance. The better dispersion of MnO_x nanoparticles over the CNTs/Ni substrate also provides a large activated surface area to the redox reaction, and consequently keeps 93% capacitance at a scan rate of 100 mV/s. The capacitive ability and reaction reversibility of the MnO_x/CNTs composite electrode in this study are better than those of other groups' reports on an MnO_x electrode.[19,20]

The electrochemical characteristics of the electrode can be realized from the electrochemical impedance spectrum and the corresponding equivalent circuit model. The ac impedance responses of the MnO_x/Ni and MnO_x/CNTs/Ni electrodes measured at open-circuit potential (OPC, ~300 mV *vs.* SCE) in 0.1 M Na_2SO_4 are shown in Fig. 7, indicating that both spectra are composed of an arc in the high-frequency region and a line in the low-frequency region. The phenomenon in the high-frequency region could be caused by the double-layer process as the response of this process is

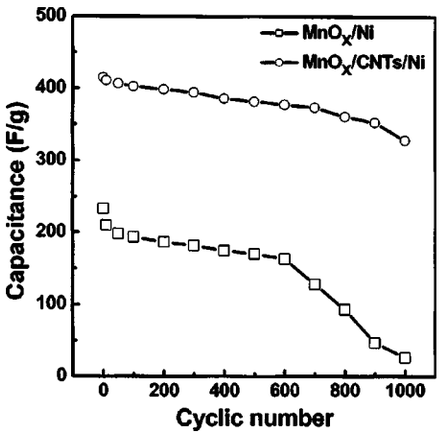

Figure 8. Stability tests of the a-MnO_x/Ni and a-MnO_x/CNTs/Ni electrodes. CV tests were measured at 10 mV/s in 0.1 M Na_2SO_4 solution.

faster than that of the faradaic process. In the high-frequency region, the intercepts with real impedance [Re (Z)] axis of MnO_x/Ni and MnO_x/CNTs/Ni are 0.863 and 0.347 Ω cm^2, respectively. This value is considered as the total electrical resistance of the electrode material (R_m), the electrolyte (R_e), and the electrical leads (R_l).[21] As the R_e and R_l are almost the same through the experiments, the decrease of total resistance could have contributed to the low resistance of the electrode materials. The electrode resistance is composed of the resistance of the electrode material and the contact resistance between materials. One can suggest that the CNTs/Ni electrode provides a rough surface and large contact area between electrode and MnO_x; therefore, the total resistance of MnO_x/CNTs/Ni becomes smaller than that of MnO_x/Ni. The imaginary part of the impedance plot of the MnO_x/CNTs/Ni electrode in the high-frequency region was larger than that of the MnO_x/Ni electrode, which is attributed to the double layer capacitor, formed by the high surface area and the well-dispersed MnO_x nanoparticles on the CNTs/Ni substrate. However, in the low-frequency region, the faradaic reaction was the main effect, as shown by the approximately linear increase in the imaginary part of the impedance spectra. The slope of the impedance plot of the MnO_x/CNTs/Ni electrode is larger than that of the MnO_x/Ni electrode as the faradaic capacitor is formed by the highly electroactive material of MnO_x deposited on the CNTs/Ni substrate. Therefore, the large surface area of the MnO_x/CNTs/Ni electrode with a high electrochemical activity exhibits better capacitance behavior.

The electrochemical stability of the electrode was investigated by applying cyclic CV measurements. Figure 8 shows the plots of the specific capacitance of MnO_x/Ni and MnO_x/CNTs/Ni electrodes *vs.* the cycle of the CV test. The specific capacitances of MnO_x/Ni fall to 83 and 70% of the original value after 100 and 600 cycles of CV test, respectively. The specific capacitance drops quickly to 11% of the original value after 1000 cycle tests. But those of the MnO_x/CNTs/Ni electrode have less reduction; the capacitances are 97 and 91% after 100 and 600 cycles of tests, respectively. The capacitance of MnO_x/CNTs/Ni remains at 79% of the original value until 1000 cycles of CV test. The CV tests indicate that the a-MnO_x/CNTs/Ni composite electrode shows good electrochemical characteristics.

Conclusions

The a-MnO_x/CNTs/Ni composite electrodes synthesized by anodic deposition at 25°C in a 0.16 M $MnSO_4 \cdot 5H_2O$ solution revealed 10-25 nm amorphous MnO_x nanoparticles on the CNTs/Ni substrate. Such nanocomposite electrodes have shown much better energy storage capabilities than those deposited on the Ni substrate, mainly due to the low resistance and large surface area of the nanocomposite electrodes. The specific capacitances of the MnO_x/CNTs/Ni electrodes were 415 and 418 F/g, as obtained from CV measurements with a scan rate of 5 mV/s and calculated from a CCD test, respectively. Furthermore, the a-MnO_x/CNTs/Ni nanocomposite electrode preserved 79% of its original capacitance in the 1000 cycles of operation. Such nanocomposite electrodes exhibit good capacitance properties and excellent reversibility. Therefore, the a-MnO_x/CNTs/Ni nanocomposite electrode may be appropriate for supercapacitor applications.

Acknowledgment

This work was supported by the National Science Council of the Republic of China, contract no. NSC 93-2623-7-009-006.

National Chiao Tung University assisted in meeting the publication costs of this article.

References

1. R. J. Brodd, K. R. Bullock, R. A. Leising, R. L. Middaugh, J. R. Miller, and E. Takeuchi, *J. Electrochem. Soc.*, **151**, K1 (2004).
2. A. Burke, *J. Power Sources*, **91**, 37 (2000).
3. Y. J. Kim, Y. Masutzawa, S. Ozaki, M. Endo, and M. S. Dresselhaus, *J. Electrochem. Soc.*, **151**, E199 (2004).
4. J. H. Jang and S. M. Oh, *J. Electrochem. Soc.*, **151**, A571 (2004).
5. A. Laforgue, P. Simon, J. F. Fauvarque, M. Mastragostino, F. Soavi, J. F. Sarrau, P. Lailler, M. Conte, E. Rossi, and S. Saguatti, *J. Electrochem. Soc.*, **150**, A645 (2003).
6. K. H. Chang and C. C. Hu, *J. Electrochem. Soc.*, **151**, A958 (2004).
7. S. L. Kuo and N. L. Wu, *Electrochem. Solid-State Lett.*, **6**, A85 (2003).
8. Q. Lin and J. N. Harb, *J. Electrochem. Soc.*, **151**, A1115 (2004).
9. S. H. Joo, S. J. Choi, I. Oh, J. Kwak, Z. Liu, O. Terasaki, and R. Ryoo, *Nature (London)*, **412**, 169 (2001).
10. K. H. An, K. K. Jeon, J. K. Heo, S. C. Lim, D. J. Bae, and Y. H. Lee, *J. Electrochem. Soc.*, **149**, A1058 (2002).
11. F. Picó, J. M. Rojo, M. L. Sanjuán, A. Ansón, A. M. Benito, M. A. Callejas, W. K. Maser, and M. T. Martínez, *J. Electrochem. Soc.*, **151**, A831 (2004).
12. E. Frackowiak, K. Metenier, V. Bertagna, and F. Beguin, *Appl. Phys. Lett.*, **77**, 2421 (2000).
13. N. Miura, S. Oonishi, and K. R. Prasad, *Electrochem. Solid-State Lett.*, **7**, A247 (2004).
14. J. A. Smith, M. Josowicz, and J. Janata, *J. Electrochem. Soc.*, **150**, E384 (2003).
15. W. Sugimoto, T. Shibutani, Y. Murakami, and Y. Takasu, *Electrochem. Solid-State Lett.*, **5**, A170 (2002).
16. J. H. Park, J. M. Ko, and O. O. Park, *J. Electrochem. Soc.*, **150**, A864 (2003).
17. R. M. Lago, S. C. Tsang, K. L. Lu, Y. K. Chen, and M. L. H. Green, *J. Chem. Soc., Chem. Commun.*, **1995**, 1355.
18. B. Gao, G. Z. Yue, Q. Qiu, Y. Cheng, H. Shimoda, L. Fleming, and O. Zhou, *Adv. Mater. (Weinheim, Ger.)*, **13**, 1770 (2001).
19. C. C. Hu and C. C. Wang, *J. Electrochem. Soc.*, **150**, A1079 (2003).
20. J. K. Chang and W. T. Tsai, *J. Electrochem. Soc.*, **150**, A1333 (2003).
21. Y. K. Zhou, B. L. He, W. J. Zhou, and H. L. Li, *J. Electrochem. Soc.*, **151**, A1052 (2004).